Biogeosciences Discuss., 12, 8573–8614, 2015
www.biogeosciences-discuss.net/12/8573/2015/
doi:10.5194/bgd-12-8573-2015

Biogeosciences Discussions
Open Access

Integrated radar and lidar analysis reveals extensive loss of remaining intact forest on Sumatra 2007–2010

M. B. Collins[1,2,3] **and E. T. A. Mitchard**[1]

[1]School of GeoSciences, University of Edinburgh, Crew Building, The King's Buildings, Edinburgh, EH9 3JN, UK
[2]Institute of Zoology, Zoological Society of London, Regents Park, London, NW1 4RY, UK
[3]Department of Geography and the Environment, London School of Economics and Political Science, Houghton Street, London, WC2A 2AE, UK

Received: 17 March 2015 – Accepted: 22 May 2015 – Published: 11 June 2015

Correspondence to: M. B. Collins (murray.collins@ed.ac.uk)

Published by Copernicus Publications on behalf of the European Geosciences Union.

Abstract

Forests with high above ground biomass (AGB), including those growing on peat swamps, have historically not been thought suitable for biomass mapping and change detection using Synthetic Aperture Radar (SAR). However, by integrating L-band ($\lambda = 0.23$ m) SAR with lidar data from the ALOS and ICESat earth-observing satellites respectively, and 56 forest plots, we were able to create a forest biomass and change map for a 10.7 Mha section of eastern Sumatra that still contains high AGB peat swamp forest. Using a time series of SAR data we estimated changes in both forest area and AGB. We estimate that there were 274 ± 68 Tg AGB remaining in natural forest (≥ 20 m height) in the study area in 2007, with this stock reducing by approximately 11.4 % over the subsequent 3 years. A total of 137.4 kha of the study area were deforested between 2007 and 2010; an average rate of 3.8 % yr^{-1}.

The ability to attribute forest loss to different initial biomass values allows for far more effective monitoring and baseline modelling for avoided deforestation projects than traditional, optical-based remote sensing. Furthermore, given SAR's ability to penetrate the smoke and cloud which normally obscure land cover change in this region, SAR-based forest monitoring can be relied on to provide frequent imagery. This study demonstrates that even at L-band, which typically saturates at medium biomass levels (ca. 150 Mg ha^{-1}), it is possible to make reliable estimates of not just the area but the carbon emissions resulting from land use change.

1 Introduction

Tropical forests provide multiple ecosystem services such as climate regulation and water filtration (Naidoo et al., 2008), yet markets fail to value them properly, leading to extensive deforestation and forest degradation (DD; Bulte and Engel, 2006). DD in developing countries accounts for between 7 and 20 % of anthropogenic CO_2 emissions e.g. 18 % (Grace et al., 2014); 15 % with range 8–20 % (van der Werf et al., 2009), 7–

BGD
12, 8573–8614, 2015

14 % (Harris, 2012). Ultimately this is leading to between 0.9 and 2.2 Pg C yr^{-1} being transferred to the atmosphere (Houghton, 2010). By contrast, the release of carbon dioxide from fossil fuel burning in the tropics is just 0.74 Pg C yr^{-1} (Boden et al., 2010), so DD dominates anthropogenic CO_2 emissions from tropical countries. Furthermore, there is extensive evidence that intact and secondary forests in the tropics are acting as a significant carbon sink, absorbing at least as much carbon dioxide than is released through tropical deforestation (Lewis et al., 2009; Grace et al., 2014). Preventing dangerous climate change will therefore be much more difficult if tropical deforestation is not reduced or reversed. DD is also leading to extensive losses of biodiversity and other ecosystem services (Koh and Sodhi, 2010). Hence there are multiple environmental benefits to be achieved by slowing or reversing these processes. Consequently, in the private sector, investors and consumers are pressurising companies trading in commodities like soy, palm oil and timber (hereafter collectively "High Deforestation Risk Commodities"; HDRC) to monitor and reduce their impact on the world's forests.

In the public and "third" sectors (Non-Governmental Organisations, NGOs) , there has been intense activity in the development of activities leading to Reducing Emissions from Deforestation and forest Degradation in developing countries, and the sustainable management, conservation and enhancement of forest carbon stocks (REDD+; UNFCCC, 2010). This currently takes the form of *inter alia* bilateral arrangements (e.g. Governments of Norway and Indonesia's USD 1bn REDD+ Letter of Intent); large multilateral programs (e.g. the UK government's GBP 3bn International Climate Fund and the World Bank's Forest Carbon Partnership Facility); and localised projects financed through the voluntary carbon market (e.g. see Diaz et al., 2011).

HDRC compliance and REDD+ may require (Task I) the quantification of above-ground forest biomass (AGB), and both will certainly require (Task II) monitoring change in forest over time. This paper addresses the technical aspects of both of these tasks, focusing on the quantification of AGB and its change over time in the same analysis. However Task II can be achieved without initially quantifying AGB (Joshi et al., 2015) e.g. measuring solely the area deforested.

BGD
12, 8573–8614, 2015

The forest areas of concern are vast and remote, necessitating the use of remote sensing (RS) techniques, typically the analysis of images captured from satellites or aircraft. With existing techniques and cloud-free optical data it is relatively simple to detect forest change. However, ideally analysts would use time series of high-resolution AGB maps (e.g. from lidar) to detect accurately DD, any forest regrowth, and quantify the associated biomass changes simultaneously. Yet there are major challenges to measuring biomass: no satellite sensor directly measures it (Woodhouse et al., 2012), and relationships between remote sensing data and biomass tend to break down at medium to high AGB levels, meaning there is a loss of sensitivity to high biomass forest (Mitchard et al., 2009a). Hence the initial AGB map (at time t_0) will contain errors, as will maps for subsequent time periods ($t_1, t_2 \ldots t_n$). Therefore detecting biomass change over time is a more troublesome proposition still, since the errors in each map must be well understood in order to be able to correctly infer their change over time. In the absence of such well-understood uncertainties, Tasks I and II must be integrated to measure AGB change. We postulate that by distinguishing between these tasks, uncertainty in the carbon stocks (typically quite high) can be separated from uncertainty in the change maps (often low). This should produce change estimates with narrower and better defined confidence intervals than those created by directly differencing biomass maps

1.1 Task I: AGB estimation

For Task 1, Mitchard et al. (2012) characterized the options available as (a) the classification of forest into landcover types, which are then attributed a mean AGB value based upon field or remote sensing measurements; or (b) the direct regression, or more complex machine-learning algorithms, between AGB measurements and a single or set of remote sensing variables. Approach (a) largely maps onto the Tier 1 and Tier 2 approaches for REDD+ monitoring proposed by the United Nations Framework Convention on Climate Change (UNFCCC).

BGD
12, 8573–8614, 2015

Tier 3, which involves local modelling, probably involves approach (b) (Arino et al., 2009). Option (a), forest classification, can be performed using the properties of sunlight reflected from the surface of the forest canopy (passive optical remote sensing; e.g. using the LANDSAT satellite series). It also can be undertaken using active sensing technologies such as Synthetic Aperture Radar (SAR) acquired at low (e.g. L-band) frequencies. Sensors operating at L-band include the ALOS-1 and ALOS-2 PALSAR-1/2. However this forest-classification approach does not reflect variations in forest within classes, leading to coarse AGB maps. Furthermore optical imagery typically suffers from interference from cloud and smoke over forest areas, hence multiple image acquisitions are required to make the final forest classification. For these reasons, option (b; direct estimation) is more attractive.

One of the most promising RS variables for option (b), direct regression, is SAR backscatter. SAR involves focusing a beam of microwave energy at the forest and using the backscattered energy to make inferences about the properties of the target. The longer (than visible light) wavelengths of SAR means that the signal does not interact with water or particulates in the atmosphere, hence it can "see" through cloud and smoke. Since the radiation interacts with the structure of the forest itself, it can be statistically related to AGB (Mitchard et al., 2012; Morel et al., 2011). However the SAR signal saturates at some level of forest biomass typically between 60 and 150 $Mg\,ha^{-1}$ for L-band, depending on the polarisation and environmental conditions (Lu, 2006; Mitchard et al., 2009a). Hence AGB modelling must either be limited at this maximum level of sensitivity, or else any pixel with AGB greater than this value can be ascribed a "high biomass forest" value e.g. as taken from forest plots. Longer wavelength SAR has potential for much higher saturation points, but no satellite collecting data longer than L-band currently exists. However, the P-band BIOMASS satellite has been funded by the European Space Agency, and should launch in 2021.

The only operational RS technology that can estimate the biomass of tropical forest without saturation at this level is Laser Light Detection and Ranging (lidar). This active sensing approach involves emitting pulses of light at a target (the forest) to determine

BGD
12, 8573–8614, 2015

structural information and thereafter AGB (Lefsky, 2010; Asner et al., 2010). Yet landscape coverage to make AGB maps is only possible using aeroplanes as the sensor platform. For instance Asner et al. (2010) measured $> 5 \times 10^5$ ha in Peru at a spatial resolution of < 1 m, yet this data needed to integrated with moderate resolution (30 m) satellite data to produce a final landscape-level map. Moreover, using aeroplanes as the platform makes data acquisition very expensive, and costs rise further due to complex data processing requirements, especially when repeated acquisition is required for monitoring. This cost representing a significant barrier to lidar's wide adoption and operationalisation as a forest monitoring tool.

Hence a monitoring problem: optical imagery typically cannot be related directly to AGB and hence relies on classification techniques, and is plagued with the problems of cloud cover. A SAR signal can penetrate cloud and smoke, increasing the regularity of usable observations (effectively whenever a SAR image is captured, compared with only a small subset of optical images). Moreover SAR backscatter can be directly related to AGB given a sufficiently long wavelength. However SAR signals saturate at AGB levels well below those found in mature tropical forests. Lidar can provide AGB estimates, yet the mapping of large areas still requires integration with other datasets.

Here we present one solution to this problem that may be implemented now, by combining the options set out above. This possibility arises because lidar footprints from the Ice, Cloud and land Elevation Satellite (ICESat) Geoscience Laser Altimeter System (GLAS) sensor provided dispersed lidar samples across the earth's surface, including over tropical forests. These data can be statistically related to – and used in conjunction with – other freely-available remote sensing data from sensors like SAR which do provide full coverage, and actively sense forest structure (Shugart et al., 2010). (This is because both approaches actively sense forest structure, measured either through differentiated laser light returns in lidar e.g. from forest floor and canopy, and in the present case, the degree of volume scattering in SAR returns). Though this lidar data is the same fundamental input, the method we propose is different to that in Saatchi et al. (2011), which involved a machine learning approach at a coarse resolution, and

BGD
12, 8573–8614, 2015

that of Mitchard et al. (2012), which uses SAR data to perform a classification and then populate the classes with AGB based on the lidar. Our approach involves two stages: direct regression for AGB mapping using a single year of SAR data, followed by an independent change detection process using multi-temporal SAR data.

Specifically, our approach is to integrate L-band Synthetic Aperture Radar (Phased Array L-band Synthetic Aperture Radar, PALSAR, $\lambda = 0.23$ m; on board the Advanced Land Observing Satellite, ALOS) with four years of data from the space-borne lidar sensor (ICESat GLAS; 10,944 footprints from 2003–2007), in order to greatly supplement a small biomass field dataset of 56 field plots. By modelling relationships between these three data sets, we are able to quantify AGB in the reference year 2007, with an increased sensitivity to higher-biomass forest than would be the case using SAR alone.

1.2 Task II: Forest and AGB change detection

For Task II, the options are to characterise the possible states of the forest system, and to measure the change in state over time. Typically this involves some form of categorising or 'binning' forest into classes. For instance an area of forest may change from intact forest to degraded forest; from degraded forest to non-forest; or from non-forest to plantation. The changed pixels can be related back to an original AGB map (if available) and AGB loss and carbon flux calculated, otherwise statistics on the areas of forest lost and degraded can be generated.

Historically such change assessments have been undertaken by using optical satellite imagery. For instance in an assessment of the impacts of protected areas (PAs) in Sumatra, Gaveau et al. (2009) used LANDSAT images from 1990 and 2000 to measure deforestation, whilst more recent efforts integrate Moderate Resolution Imaging Spectroradiometer (MODIS) data in addition to LANDSAT. Broich et al. (2011a) used this combination to map forest change across Sumatra and Kalimantan. This work highlighted the central problems both of identifying forest type from optical remote sensing imagery, and the use of composite images from several different time periods. Composites are necessary when clouds obscure parts of the study area in the first image

BGD
12, 8573–8614, 2015

collected; using cloud-free sections of later images ultimately allows the creation of a largely cloud-free image. Yet cloud-free imagery for those areas obscured in the first image may not be available for months or even years after the first image is collected. Since forest is being cleared and replaced with plantations very rapidly in places like Indonesia, this means that composite images do not incorporate the deforestation and regrowth that has occurred in the time period during which the composite was created (Hansen et al., 2008, 2009). Change detection based on these composites may therefore underestimate the extent of forest change. One solution is to use algorithms to develop pixel forest histories (Broich et al., 2011b), yet this approach seeks a solution more in inference than in data. A more recent Sumatra-wide study using LANDSAT and lidar, Margono et al. (2012) re-iterates these interacting monitoring challenges of high cloud cover and rapid regrowth. Nonetheless, optical data has been used to produce impressive multi-year global forest change products across habitat types (Hansen et al., 2013).

Our novel solution for Task II is to use inter-annual threshold-delimited differencing of L-band SAR data to provide annual DD estimates. We use these changes in conjunction with the map produced as a solution for Task 1, in order to measure AGB loss, and estimate CO_2 emissions. We test this approach for a section of Sumatra, Indonesia. This is an ideal study site because Indonesia has an extremely high deforestation rate, which reached 2 Mha yr^{-1} in 2011 to 12 (Hansen et al., 2013). Simultaneously there is considerable action to being taken to address this including the proliferation of REDD+ and HDRC monitoring activity, for instance with Norway committing $1bn to a bilateral REDD+ deal (The Norwegian Embassy, 2011; Solheim and Natalegawa, 2010), and via the Round table on Sustainable Palm Oil, (RSPO).

BGD
12, 8573–8614, 2015

2 Methods

2.1 Field Site

Our forest plot data are from Berbak National Park (BNP; 104°20′ E; 1°27′ S), a peat swamp in Jambi province, Sumatra, covering 140 000 ha. It is habitat for the Critically Endangered Sumatran tiger (*Panthera tigris sumatrae*, CR; IUCN, 2013) and 23 species of palms, making it the most palm-rich peatland swamp known in SE Asia. The Zoological Society of London (ZSL) has established a pilot REDD+ project here known as the Berbak Carbon Initiative (BCI), managed in partnership with the Government of Indonesia (GoI). However since the SAR data for this study were available at a far larger extent than that of the project site, we expanded the analysis to a scene which covered portions of both Jambi and South Sumatra provinces, covering 10.7 Mha. A map of the study area is provided in Fig. 1.

These provinces were once entirely covered by mega-diverse Sundaland lowland rainforest, supporting *inter alia* the world's largest (*Rafflesia* sp.) and tallest (*Amorphophallus* sp.) flowers; the Sumatran rhinoceros (*Dicerorhinus sumatrensis*), and stands of Ironwood (*Eusideroxylon zwageri*; Whitten et al., 1984). The forest types range from mangrove forest; lowland peat swamp forest; lowland *terra firme* forest; through to hill and montane forest in the Bukit Barisan mountains (*ibid*). However this description is now largely historical: the expansion of industrial logging, followed by transmigration of Javanese settlers; and oil palm (*Elaeis guineensis*) plantation development has led to extensive DD e.g. (Whitten et al., 1984; Gaveau, 2013; Broich et al., 2011a, b; Miettinen et al., 2011). Hence anthropogenic land cover is increasingly dominant, in particular with oil palm and "fastwood" (*Acacia* sp.) plantations expanding to meet international food, energy and wood pulp demand; whilst coconut plantations have expanded along the coastline.

Using land-use planning GIS shapefiles provided by the Indonesian government to ZSL, we calculated that 1 % of the area is designated as community forest; 26 % as production forest; and 10 % protected forest. The majority is designated for non-forest

BGD
12, 8573–8614, 2015

use (60 %) e.g. for cities and agriculture. It should be noted that these are aspirant land use designations: their implementation in Indonesia is complicated (Collins et al., 2011).

2.2 Field plot data

ZSL undertook a carbon stock assessment during the initial phase of the REDD+ pilot project. This involved including forest AGB estimation using forest plots. Plot locations were chosen through stratified random sampling, based upon a habitat classification map using 2008 SPOT V imagery analysed by ZSL Indonesia. In the field, plot locations were verified with a Garmin 60CsX handheld GPS unit. A total of 56 plots were sampled, with 36 in primary swamp forest, 14 in swamp bush and 6 in secondary peat swamp forest. The plots were nested, constituting:

1. The main plot of 20 × 125 m plot recording stem ≥ 1.05 m circumference
2. a 20 × 20 m sub-plot recording stems > 0.30 m and < 1.05 m circumference
3. a 10 × 10m subplot recording stems ≥ 0.15 m and ≤ 0.30 m circumference.

The AGB for each tree in each sub-plot was then calculated using an allometric equation for wet tropical forests, where:

$$\mathrm{AGB} = \exp\left(-2.557 + 0.940 \times \ln\left(\rho d^2 \eta\right)\right) \quad (1)$$

where ρ = oven-dry wood over green volume (wood density), d = diameter at breast height (1.3 m), η = tree height (Chave et al., 2005). Wood densities were collected from the literature for Indonesia peat swamp trees (Murdiyarso et al., 2010). There were no palms recorded in the plot data, yet they may be among the 5.3 % of the stems that were unidentified by the field team. Future research may identify these species and identify specific allometric equations and wood densities. However for the present analysis, we followed the Food and Agriculture Organisation recommendation of the

BGD
12, 8573–8614, 2015

use of an arithmetic mean for tree wood density where trees are not individually identifiable in the field plots. This is 0.57 g cm^{-3} for Asia (Reyes et al., 1992), or a generic 0.58 g cm^{-3} (Chave et al., 2004). We used the former figure.

2.2.1 Calculating tree height

Tree height data was not recorded from the forest plots by the field team. Equations published by Morel et al. (2011) were therefore used to relate tree height to DBH for S.E. Asian trees, whereby height η:

For stems where $d < 20$ cm:

$$\eta = 8.61 \times \ln(d) + (-8.85) \quad (2)$$

and where $d > 20$ cm:

$$\eta = 16.41 \times \ln(d) + (-33.22) \quad (3)$$

where d is diameter at breast height. The estimated height for each stem was then used to calculate Lorey's height (L) for each of the plots. We did this because L is the closest to what the ICESat GLAS waveforms measure (Lefsky, 2010). Lorey's height weighs the contribution of trees to the stand height by their basal area. It is calculated by multiplying tree height η by its basal-area α, and dividing the sum of this by the total stand basal area.

$$L = \frac{\sum(\eta \times \alpha)}{\sum(\alpha)} \quad (4)$$

2.2.2 Estimating the relationship between the measured biomass and height

The next step was to calibrate the relationship between plot-level AGB estimates and Lorey's height estimated in the steps above. This involved following the approach of Saatchi et al. (2011) and Mitchard et al. (2012), which is to estimate a non-linear least-squares regression: $y = a \times (x^b)$. We estimated this using the NLS function in R (R Core Team, 2013).

BGD
12, 8573–8614, 2015

2.3 SAR and lidar data

We downloaded ALOS-PALSAR mosaics from 2007 to 2010 from the Japanese Aerospace Exploration Agency (JAXA) website (JAXA, 2014). The Polarimetric L-band Phased-Array Synthetic Aperture Radar (PALSAR) data are collected in two polarisations: Horizontal-send Horizontal-receive (HH) and Horizontal-send Vertical-receive (HV), and is provided at 25 m resolution. We aggregated this by taking the mean of a 4 × 4 pixel window, as an initial multilooking procedure to reduce speckle. Since an initial change detection produced noisy images, we then used an Enhanced Lee filter with a 3 × 3 window on each of the now 100 m HH and HV rasters, using ENVI (Exelis) and the default parameters.

Lidar data were taken from the ICESat GLAS sensor. These data were collected between 2003-2007, and provide waveforms for transects across the earth's surface. The final data used here were the estimates of Lorey's height from each waveform derived from coincident tropical ground data, as used by Saatchi et al. (2011). On examining the data in a GIS, there were clearly many footprints over areas that were known to be covered in forest (from field observations) but that were influenced by smoke and cloud cover because they had Lorey's height values of 0 m. To deal with this we filtered the lidar footprints for any false negatives, using an independent land cover data set from the European Space Agency (ESA) called GLOBCover (Bicheron et al., 2009). This provides estimated land cover type across the study area, and at 300 m resolution it is the highest resolution land cover data available. We then removed lidar footprints from the dataset which had Lorey's height values of 0 m but which were over forest in the GLOBCover data. By this process 11 031 lidar footprints were removed, leaving 10 944 points remaining for calibrating the SAR data.

BGD
12, 8573–8614, 2015

2.4 Calculating natural forest AGB stocks

2.4.1 Calibration of SAR and lidar data: creating a forest height map

For 2007 we calibrated the SAR data in decibels (dB) with the lidar data by modelling a functional relationship between the Lorey's height measurements and the HV backscatter value of the pixels in which the lidar footprints fell.

However lidar data over this type of mixed and degraded forest landscape typically contains far more data points at lower values of Lorey's height, with very few readings greater than 30m. Yet for an ideal regression a similar number of Lorey's height estimates are necessary at all SAR backscatter levels. Therefore we binned the data, whereby we calculated the mean backscatter at each Lorey's height interval (1, 2, 3...25 m) using the aggregate function in R (R Core Team, 2013).

A physical limitation of the L-band SAR data is that it does not fully penetrate the forest canopy, and the signal saturates at higher biomass levels (Mitchard et al., 2009a, 2011). This is demonstrated by a change in the functional relationship between the Lorey's height measurement from lidar and the HV backscatter, which occurs at approximately 25 m Lorey's height in this instance, corresponding to 190.6 Mg ha^{-1}, and as shown in Fig. 3. Therefore we modelled the relationship using a non-linear regression estimated in R, taking the natural logarithm of the Lorey's height i.e.

$$\mathrm{HV} = \ln(\mathrm{Lorey}) + e \quad (5)$$

The relationships using the HV backscatter were superior to those developed using the HH backscatter, and so we continued the analysis using only this polarisation (e.g. Mitchard et al., 2009b).

We then applied the functional relationships between backscatter and Lorey's height to the 2007 HV backscatter raster using equation 1. In practice this meant calculating Lorey's Height L using:

$$L_{2007} = e^{\left(\left(\mathrm{HV}^{\mathrm{dB}}_{2007}+\alpha\right)/\beta\right)} \quad (6)$$

BGD
12, 8573–8614, 2015

This created a map for 2007 which estimated Lorey's height per pixel.

2.4.2 Excluding agriculture and plantations from the Lorey's height map

Since our analysis concerns the loss of natural forest only rather than AGB in all land cover types, we excluded those pixels which had a modelled lorey's height < 20 m from the subsequent analysis. We considered that trees at this height would be natural forest rather than plantation. Further, our model estimates that forest 20 m high has AGB of 123.7 Mg ha^{-1}, whereas a study on neighbouring Borneo also using ALOS PALSAR found that the mean biomass of plantations was 53 Mg ha^{-1}, with values above this on average representing natural forests (Morel et al., 2011). So by choosing this forest height limit of 20 m hence AGB 123.7 Mg ha^{-1}, we greatly increase our confidence that we have excluded plantations from our maps, and hence also plantation cropping cycles in the subsequent change analyses. We also deemed our restriction to be in keeping with the definition of "forest" under the Marrakesh Accords (UNFCCC, 2001).

Next we undertook spatial filtering. We wrote a bespoke moving window in *R* based on the focal function from the raster package (Hijmans, 2013), and applied it to the 2007 Lorey's height map. For each 5 × 5 pixel window, if ≥ 20 (80 %) of the pixels were estimated to contain forest of ≥ 20 m lorey's height, we included all of those pixels in the subsequent analysis. Otherwise, if < 20 pixels were estimated as forest, we excluded all these pixels. This will result in the exclusion of small patches of remnant natural forest, hence ultimately to underestimation of the 2007 AGB stocks. However, it allows us further to increase our confidence that we are excluding plantations from the analysis, and allows us to focus instead upon mapping the biomass and the deforestation of Sumatra's last intact contiguous high biomass forest. Visual comparisons of the resulting map with GoogleEarth data and our own field knowledge suggested that these processes had indeed masked out plantations without removing any large areas of natural forest.

BGD
12, 8573–8614, 2015

2.4.3 Creating the 2007 biomass map

In order to create the final biomass map for 2007, we applied the relationship between Lorey's height and forest plot biomass (Eq. 10) to the Lorey's height raster created above. We processed all data with UTM projection (48S) at 100 m resolution in order to readily calculate biomass stocks per hectare.

To account for the saturation of the HV backscatter signal and hence functional relationship at this point, we limited the modelled biomass estimate at 196.6 Mg ha^{-1}. For any pixel >196.6 Mg ha^{-1}, we attributed a mean biomass value taken from the Berbak forest plots with >25 m Lorey's height. This was 236.5 Mg ha^{-1} ($n = 8$; SD = 75.7 Mg ha^{-1}). This figure is more conservative than the generic 350 Mg ha^{-1} for Asian forests as suggested by the IPCC (Eggleston et al., 2006; Penman et al., 2003).

2.5 Calculating errors and uncertainties

In a study estimating biomass there are a combination of random and systematic errors propagating throughout the calculations. Mitchard et al. (2011) characterises the errors as those concerning (a) accuracy and (b) precision. Accuracy concerns the distance of the mean from the true value and hence systematic biases. Precision concerns the distance of a measurement from the mean of multiple measurements of the same attribute and is this due to random errors. In a comprehensive review of errors in biomass estimations, Chave et al. (2004) highlight how in practice these errors can occur when for instance taking the measurements of the individual trees themselves; random errors in the identification of tree species; spatial errors relating to geo-location.

We considered each of the potential sources of error in turn, namely those deriving from the binary forest map from the ESA; the tree species identification, and height and AGB estimations; errors in the lidar data and Lorey's height estimates; and the relationships estimated between lidar and SAR backscatter. In order to combine these multiple errors, which we assume to be uncorrelated, we used the following formula to

BGD
12, 8573–8614, 2015

determine uncertainty (U; Saatchi et al., 2011):

$$U_{\text{total}} = \sqrt{U_1^2 + \ldots\ldots + U_n^2} \quad (7)$$

2.6 Deforestation detection

2.6.1 Radiometric normalisation of the 2008 : 2010 HV backscatter rasters to the 2007 dataset, and additional processing

Annual variations in measurement conditions, such as moisture on the ground and in vegetation introduces variance in backscatter between years which does not constitute changes in forest state. In the wet tropics these changes can be large. For change analysis this represents a problem. Any differencing between data sets over time for change detection could result in errors whereby backscatter changes reflect differences in moisture rather than real changes in the forest. In order to correct for this, the data needs to be radiometrically normalised such that the measured properties of a pixel in year t_0 approximate the properties of the pixel in year t_1 where no land use change has occurred. In order to do this with the SAR data, we randomly extracted 25 000 pixels from all four HV backscatter mosaics from 2007 : 2010. We used these data to develop a linear relationship between each pixel over time, using a Reduced Major Axis Regression model estimated in R (Legendre, 2014), and assuming that any sampled pixels which deforested during the study period would constitute errors in the regression. We applied the resulting relationships to the 2008 : 2010 data so that the mean backscatter of each scene approximated that of 2007.

Finally, the data provided by JAXA is already terrain-corrected and provided in Gamma nought (Γ^0) geometry. Hence we did not apply any further terrain correction.

2.6.2 Exclusion of flooded areas

Seasonal flooding can cause changes in SAR backscatter that could subsequently be misinterpreted as deforestation, that is unlikely to be corrected using radiometric cali-

BGD
12, 8573–8614, 2015

bration. Flooded forest has high backscatter values in the Horizontal send, Horizontal receive (HH) polarisation relative to the Horizontal send Vertical Receive (HV) polarisation. This is because in the HH polarisation, there is a double bounce of the SAR signal between the water surface and the structure of the forest which increases the HH backscatter value relative to HV. So flooded forest can be detected by looking at changes across space in the ratio of these two polarisations. We excluded any areas identified as natural forest (calculated in the section above; ≥ 20m height but which had an HH value of > −5 dB. These excluded areas appear as white "ribbons" through the in-tact forest blocks in Fig. 4, alongside the region's rivers. Additional visual verification of the efficacy of the approach is provided in Fig. S1 in the Supplement.

2.7 Change detection: the determination of deforestation

In order to determine deforestation we calculated the difference in Lorey's height for each time step: 2007–2008; 2008–2009 and 2009–2010. We used the Lorey's height maps for two reasons. First, the relationship between Lorey's height and HV backscatter is non-linear. Hence the change in backscatter in a pixel implies a change in Lorey's height and therefore forest state that is conditional upon the original backscatter value of that pixel. This means it was not possible to simply take a difference in the HV backscatter between years to detect change. Second, forest height is a more intuitive property than HV backscatter.

Whilst there is small-scale degradation in addition to deforestation at the study site, we are concerned here with land use change as a binary, exclusive event in natural high biomass forest. The threshold we used to define change between years represents a tradeoff between sensitivity and uncertainty. The lower the threshold for change detection, the more sensitive the process is. However, the more sensitive the process is, then the greater the chances that SAR speckle is detected as false positive deforestation. Ultimately we used a threshold of 10m reduction in lorey's height per pixel per year to indicate deforestation. This is because a change of this magnitude in a pixel we had assessed to be natural, non-flooded forest in 2007, would necessarily reflect a move-

BGD
12, 8573–8614, 2015

ment from high HV backscatter, high lorey's height and high biomass (i.e. intact high biomass natural forest), to a low backscatter value associated with low lorey's height and low biomass (deforested pixel). This explanation is more readily understood with reference to Fig. 3.

In practice, to detect change, we had to both calculate a series of Lorey's height maps, and account for how the errors in the HV Lorey's height relationship would propagate into the change maps. First, to produce Lorey's height maps for each year, we applied Eq. (6) to each of the radiometrically corrected annual SAR scenes 2008,9 and 10. We then considered the proportional errors (δ; ratio of regression error RMSE to maximum height estimated, 25 m) in the relationship between HV backscatter and Lorey's height. To be conservative, for each time-step, we calculated the minimum estimated Lorey's height for time t ($L_{t^{\min}}$) , and from this subtracted the maximum estimated Lorey's height for $t+1$ ($L_{t+1^{\max}}$). We calculated the minimum Lorey's height estimate by multiplying the Lorey's height estimate map by $1-\delta$, and maximum by $1+\delta$.

Therefore the forest height change (ΔL) calculation for a given time-step was:

$$\Delta L = (L_{t^{\min}}) - (L_{t+1^{\max}}) \tag{8}$$

We may now substitute in Eq. (6) for each of the Lorey's height estimates and apply the minimum and maximum error calculations:

$$\Delta L = \left(\left(e^{\left(\left(HV_t^{dB}+\alpha\right)/\beta\right)}\right) \times (1-\delta)\right) - \left(\left(e^{\left(\left(HV_{t+1}^{dB}+\alpha\right)/\beta\right)}\right) \times (1+\delta)\right) \tag{9}$$

This provided change maps between 2007 and 8; between 2008 and 9; and between 2009 and 10. Once a pixel had been detected as deforested or heavily degraded, it was excluded from consideration in the next time-step.

In summary, a pixel was only classified as having lost forest if it originally had forest ≥ 20 m height in 2007; and was not flooded (exclude HH > -5 dB); whose height was reduced by $>(10$ m) in the subsequent year; and if it had not experienced deforestation in any of the previous time periods.

BGD
12, 8573–8614, 2015

3 Results

3.1 The relationships between Lorey's height and forest plot biomass

The forest plot data from Berbak national park yielded a power relationship between estimated values of Lorey's height and AGB, which explained almost two-thirds of the variation in the data ($R^2 = 0.61$; RMSE = 113 Mg ha^{-1}). The plot data range from those with very few trees and hence low AGB and Lorey's height values, through to the primary forest plots of AGB > 300 Mg ha $^{-1}$ and Lorey's height values of ≈ 30 m. The resulting equation is shown in Eq. (10), and is plotted in Fig. 2.

$$\mathrm{AGB} = 0.37L^{1.94} \quad (10)$$

3.2 The relationship between SAR HV backscatter and Lorey's height from lidar

The relationship between HV backscatter and Lorey's height appears to be approximately linear from very low values of Lorey's height clustered at a mean of ≈ 0 m through to high values of ≈ 25 m. Figure 3 illustrates this relationship. Values in the upper-right portion of the graph have both high Lorey's height values and high HV backscatter values. We interpret these as representing mature forest with high AGB. In the bottom left of the graph are data points which have low AGB and low Lorey's height values, which we interpret as being deforested.

This graph is also central to the change detection procedure since it demonstrates the logic behind the choice of the 10m height change threshold. If a pixel with forest ≥ 20 m in t (top right of graph) experiences a height reduction of > 10 m in time $t + 1$ (moves to the lower-left of the graph), we interpret this as a deforestation event (though note Eq. (9) which illustrates how we deal with error propagation). This is the deforestation process with respect to HV backscatter and is represented by the arrow pointing downwards to the left. The functional form of this relationship is summarised in Table 1.

BGD
12, 8573–8614, 2015

3.3 Forest biomass stocks

Integrating the field plot data, the Lorey's height data and the HV backscatter data; and excluding flooded forest pixels, and summing the stocks across all the 100 m × 100 m pixels produces an estimate of 274 Tg AGB in natural forest ≥ 20 m in height across the 10.7 M ha study area in 2007. We provide an AGB and uncertainty map in Fig. 5. Relatively little of this forest type remained in 2007, and what did still remain was highly fragmented. The largest block of remaining intact forest in the study area was Berbak National Park/BCI in the north-east tip of the scene. The large treeless area in the centre of the park in this image is a burn scar from the devastating El Niño fires of 1996/1997.

3.4 Change detection and AGB loss

Our analyses suggest that a total of 137,367 1 ha pixels were deforested between 2007 and 2010 in our study area. This represents a loss of 11.4 % of the 2007 high biomass forest cover, a mean deforestation rate of 3.8 % yr^{-1}. This deforestation constitute a loss of 11.3 % of the 2007 AGB. The figures differ since not all (89 %) of the deforested pixels were in the highest biomass forest of 236.5 Mg ha^{-1}. This suggests first that deforestation is occurring in different forest types, both in the last remaining old-growth high-AGB forest, and in the lower-AGB intact forest (the minimum forest height we consider is 20 m; 123.7 Mg ha^{-1}). Second, a visual inspection of the patterns of forest loss suggests two different types of deforestation across space. The first may be characterised as scattered losses in forest that was already highly fragmented in 2007. We suggest that this represents clearance by small-scale loggers and farmers. This kind of deforestation is typified by the forest lost between 2007–2008 in the central-southern part of Fig. 4b. The second type of deforestation we observe is large-scale geometric patterns, which we suggest are characteristic of timber concessions developement and their conversions into plantations, a process via which virtually all AGB is removed. This is typified by Fig. 4c. In the west of this image, we observe forest clearance which

BGD
12, 8573–8614, 2015

advances into the remaining natural forest in annual waves from 2007–2010, which we visually verified using high resolution imagery from 8 May 2009 in GoogleEarth at 1°53′40.71″ S, 103°52′56.69″ E, as shown in Fig. 4d. In 2008–2009 we observe the construction of a road or canal which links two newly-cleared areas diagonally (south-west of Fig. 4c, zoomed in 4e). This particular image demonstrates well the level of detail which is possible to map using this approach. Discussions with the ZSL team suggest that the deforestation in the east of Fig. 4c is the result of a road building project linking Jambi to South Sumatra, the area surrounding which is also beset by illegal logging.

Berbak national park is experiencing no large scale deforestation, however the maps do show more scattered pockets of small scale forest loss which are more typical of the creation of small fields and small-scale illegal logging operations that affected many of Indonesia's national parks during the study period (Collins et al., 2011).

By aggregating all the changes across the scene we were able to estimate the total amount of AGB removed from the study area annually. We also provide potential emissions from this loss of AGB, based on an extreme scenario in which all the AGB was completely oxidised following its removal from the landscape. However, there are uncertainties involved in these calculations. Their estimation and subsequent integration into the final results are discussed below.

3.5 Errors and Uncertainties

3.5.1 Binary forest map from ESA

We used a binary forest/non-forest map from the 2005 ESA Globcover (MERIS) to remove lidar points which suffered cloud and smoke interference. This had the potential to cause three potential problems: (1) this land cover classification contains errors, which are introduced into lidar-backscatter relationships for non-forest vegetation. Indeed the classification's creators describe forest area overestimation where data are poor (Bicheron et al., 2009); (2) The lidar data were collected between 2003 and 2007,

BGD
12, 8573–8614, 2015

and so overlap the MERIS dataset. Nonetheless, given the rate of change observed in this study, land cover change could have occurred between the collection of the two datasets; (3) The GLOBCOVER data has a relatively coarse resolution of 300 m, meaning some non-forest areas will have been classified incorrectly as forest and vice versa. Artefacts relating to these errors will increase noise in the relationship shown in Fig. 3, but should not change the absolute relationship which is dominated by the signal in the data. We do not believe that these errors are significant, see Fig. 3 for the clear relationship between lidar-derived lorey's height and HV backscatter, with the fit having an R^2 of 0.91.

3.5.2 Tree species identification, height estimations and AGB estimations on forest plots

Tree identification is an ongoing endeavour in Indonesian peat swamp forests. Accordingly the field team botanist had difficulty identifying some tree species (5.3 % stems). Hence it was not possible to specify wood densities for these individuals. We would be able to increase the accuracy of the biomass map were improved tree identification and wood densities to become available. In addition the forest plots data did not contain tree height measurements, requiring using a published height to DBH relationship for S.E. Asia from Morel et al. (2011). Yet morphological differences between peat swamp trees and those measured by Morel may introduce errors into our biomass estimations. In addition the model for stems where $d < 20$ cm was poor with an R^2 value of only 0.16. This means that the predictions for the smaller stems are likely to have quite low accuracy, which is expected to have introduced further errors into the estimates of height. However the majority of forest biomass is typically found in large trees (Slik et al., 2013), rendering this problem marginally important. Nonetheless, more forest plot data that included tree height measurements would improve our calibrations. A final issue is that in order to calculate AGB, it was necessary to use pan-tropical rather than regional allometric equations. In order to account for these errors, we ascribe 20.3 % error to potential differences in regional estimates of biomass (Djomo et al., 2010).

BGD
12, 8573–8614, 2015

3.5.3 Lidar and Lorey's height estimates

The relationship that was used to develop estimates of Lorey's height from lidar returns is based upon field plots in the Amazon (Lefsky, 2010). To deal with the errors that this will create, a 5 % error is ascribed to potential differences in regional estimates of Lorey's height from the waveforms as suggested by Mitchard et al. (2012).

3.5.4 Relationship between lidar and SAR backscatter

There are errors in the estimated relationship between the estimated Lorey's height and SAR backscatter. The Root Mean Squared Error was used to quantify this, which is a measure of the difference between the values implied by an estimator in a statistical relationship and the true value of the parameter being estimated. For the relationship estimated between the 2007 HV backscatter data and the Lorey's height data, the RMSE is 3.3 m. We calculated the percentage by dividing 3.3 by 25 m (the maximum height we used from the lidar data) × 100 = 13.2 %.

3.5.5 Combining uncertainties, and final forest change results

With 20.3 % error for the biomass calculations for the trees and 5 % Lorey's height errors, and 13.2 % error for the relationship between Lorey's height and HV backscatter, we estimate 24.7 % total uncertainty using Eq. (7). We applied these uncertainties to the biomass and change calculations to produce the final results :

- 2007–2008: 27.7 kha forest containing 6.3 ±1.6 Tg AGB cleared; 2.3 % of the 2007 AGB total; potential emissions of 11.5 ± 2.9 Tg CO_2e.
- 2008–2009: 75.3 kha forest containing 16.9 ±4.2 Tg AGB cleared; 6.2 % of the 2007 AGB total; potential emissions of 30.9 ± 7.7 Tg CO_2e.
- 2009–2010: 33,955 kha forest containing 7.8 ±1.9 Tg AGB cleared; 2.8 % of the 2007 AGB total; potential emissions of 14.2 ± 3.5 Tg CO_2e.

BGD
12, 8573–8614, 2015

We illustrate the uncertainty in the AGB map in Fig. 5.

3.6 Calibration over space

We calibrated the SAR data using ground plots from the peat swamps of Berbak. However, the relationship may differ in other forest types type, and so the analysis may be enhanced by having calibrations in different areas by partitioning the backscatter data and using additional regional plot data. However, in the absence of additional forest plot data sets this was not possible.

3.6.1 Detecting biomass in mangrove forests

Not all ecosystems are equally well detected by SAR. An extensive mangrove forest south of Berbak (Sembilang National Park) appeared to have very low biomass in the biomass map. This may be because Mangrove forest's low, open canopy and extensive prop root networks absorbs much of the L-band radiation. There is even evidence that the relationship between AGB and HH backscatter is negative (Cohen, 2014). Our study therefore likely misrepresents biomass in Sembilang.

3.6.2 Underestimation of biomass loss overall

The biomass loss and emissions estimates provided are conservative. First, the maximum biomass estimate of mature forest is limited, due to SAR backscatter saturation. Second, mangrove forest biomass is underestimated. Third, the large below ground biomass emissions associated with the clearance of forest on peat soils are not included (Page et al., 2002). Fourth, the forest plots from Berbak are not likely to be representative of all the forest types across Sumatra. Fifth, we apply a very restrictive threshold of forest > 20 m height, plus a majority-value window to focus solely on the intact high biomas forests in the change analyses. Therefore we strongly expect the true carbon loss values to exceed those given here, by an undetermined amount. The bottom of our confidence intervals should be considered as the minimum emissions

BGD
12, 8573–8614, 2015

that have resulted from this land-use change, and provide a conservative estimate that could be used in a GHG accounting framework.

4 Discussion

We have demonstrated for the first time that it is possible to employ use a fusion of SAR, lidar and forest plot data to map AGB and its change across a tropical forest landscape. From a broader perspective our findings have implications (a) for forest monitoring technology and methodologies, and (b) for *inter alia* biodiversity and ecosystem services, particularly climate regulation.

4.1 A: Forest monitoring technology and methodologies

Concerning the first set of issues, our results demonstrate the value of integrating multiple existing datasets in order to map AGB in an area with high biomass forest, including peatlands. This was enabled by the establishment of robust relationships between (i) AGB and Lorey's height estimates from forest plots and (ii) HV backscatter and Lorey's height estimates from lidar data, which increases by two orders of magnitude the number of observations of Lorey's height which we have from the 56 forest plots alone.

Rapidly changing forest provides a challenging context for analysis: the deforestation rates we observed would appear to substantiate the concern that multi-year optical composites to remove cloud cover may mask the very changes that the researcher intends to detect in the first instance (Hansen et al., 2008, 2009). Hence our approach may be used either as an alternative to traditional optical analyses, or as a complement for those areas particularly affected by cloud and smoke.

Examining the per-pixel HV backscatter values over time allowed us to make spatially explicit estimates of forest biomass loss annually, and with quantified uncertainties. This represents a methodological deviation from the work to map deforestation using optical data. This provides a contribution to the call for accurate forest monitoring

BGD
12, 8573–8614, 2015

data for Indonesia to contribute to REDD+ (Broich et al., 2011a). Being able to directly map biomass at 100 m spatial resolution unencumbered by cloud or atmospheric particulates represents a significant advance in the ability to monitor tropical forests for many stakeholders, and should be of interest to governments as well as firms in HDRC sectors, and NGOs interested in forestry.

Nonetheless there are some technical barriers to continued efforts using the methodology we present. Principally, following the failure of the sensor on ALOS1, L-band SAR data was not collected again until 2014 with the launch of ALOS2, leaving a three-year data gap. Nonetheless, whilst browsing the LANDSAT archives for images of Berbak, the majority of images were obscured by cloud and smoke, meaning that despite the data gap from ALOS being sub-optimal, it is nonetheless comparable with LANDSAT data over that same period.

Finally, the estimation of per-pixel biomass requires contemporaneous lidar data for calibrating the AGB map. However the only freely available data set (ICESat) stopped collecting data in 2007. Yet plans are afoot for the deployment of ICESat 2 and GEDI which will allow calibration of future SAR images. Furthermore, demand for forest monitoring has spurred a development in other options, particularly aerial lidar transect sampling. This takes the same approach as ICESat, using lidar as a sampling tool only, recording data in transects rather than across the landscape. This offers some of the benefits of landscape level lidar mapping, by enabling providing accurate biomass estimations for different forest types, but with lower costs since only transects are recorded. Such data could be used as an alternative to ICESat 2 data, to calibrate L-band data to produce AGB maps. In addition, future work may not be restricted to ALOS2 data, with Argentina's SAOCOM and NASA's NISA L-band satellite planned for launch during this decade. These additional satellites may increase data availability and frequency of observations.

BGD
12, 8573–8614, 2015

4.2 B: Significance of deforestation and forest degradation on Sumatra

Concerning the second set of issues, our results have broad implications. Indonesia is already well-known to have very high deforestation rates. However, even in this context, forest loss in Sumatra is particularly high. By 2010, the eastern regions of Sumatra had lost approximately half of the peat swamp forests existing a decade earlier, an extremely high loss rate of 5 % yr^{-1} (Miettinen et al., 2011). In one case in June 2013, 140 000 ha of forest were destroyed by fire in a 3.5 M ha area in Riau province (Gaveau, 2013). Even on the conservative and unlikely assumption that the entire area was forested previously, this represents the extraordinary loss of 4 % of the remaining forest in a single month. Our results serve to confirm these findings: the high national means of forest loss in Indonesia mask remarkably high losses on a local scale.

Such extensive forest loss on Sumatra is having large impacts on biodiversity losses. Flagship species like tigers (*Panthera tigris sumtrae*) are Critically Endangered (IUCN, 2013). Even a decade ago, tiger biologists were already concerned about tigers being scattered as meta-population living in increasingly disconnected forest fragments (Linkie et al., 2006): the rapid deforestation we have observed thus simply represents a ongoing and unmitigated trend in habitat loss. Our maps show how very little high biomass natural forest now remains in this part of Sumatra.

As Sumatra's forest is cleared, there are huge associated CO_2 emissions both from fires and organic decomposition of AGB, but also from below ground biomass. These emissions are particularly high in the eastern Sumatran lowlands due to the presence of a blanket of peat which may contain an order of magnitude more carbon than the forest growing on it (Page et al., 2002; Jaenicke et al., 2008; Hooijer et al., 2010, 2012). Hence there is a spatially explicit issue: deforestation in peat swamps is likely contributing disproportionately highly to climate forcing than forest loss elsewhere, with peatland drainage and oxidation now accounting for up to 3 % of total anthropogenic CO_2 emissions (van der Werf et al., 2009).

BGD
12, 8573–8614, 2015

Optimistically, the increase in the range of technologies available to monitor forest, including peatland forest, irrespective of cloud and smoke cover may go some way to improving the transparency and sustainability of land use management practices. For instance, better data may contribute to the monitoring and verification of pulp paper, and oil palm firms' commitments to zero deforestation, hence mitigating some of the impacts of the very rapid environmental change we have quantified here.

The Supplement related to this article is available online at doi:10.5194/bgd-12-8573-2015-supplement.

Author contributions. M. B. Collins wrote the R code, undertook the analysis and prepared the manuscript. E. T. A. Mitchard contributed to the analyses and writing, and processed the SAR data.

Acknowledgements. ZSL Indonesia kindly hosted M. B. Collins in Indonesia. ZSL Indonesia collected the Berbak forest plot data. M. B. Collins gratefully acknowledges a PhD scholarship from the NERC-ESRC which supported this work. M. B. Collins is currently funded by Innovate UK (grant ref:TS/L007037/1) and the Natural Environment Research Council (grant ref: NE/M021998/1). The Grantham Research Institute on Climate Change and the Environment at the LSE kindly hosted M. B. Collins during his PhD. Processed GLAS data was provided by S. S. Saatchi, NASA JPL. The raw ICESats GLAS data were processed and provided by NASA and NSIDC. ALOS PALSAR data were provided free of charge by JAXA and METI through the Kyoto and Carbon Program, and we also acknowledge the support of JAXA's 4th research announcement. We acknowledge the permissions and documentation granted by the Indonesian Government, including The Indonesian Academy of Science (LIPI), and Research Council (RISTEK). We also thank the national and regional offices of the Government of Indonesia and particularly the Ministry of Forestry for all their vital support, and facilitation of ZSL's work in Indonesia. Mandar Trivedi and Sassan Saatchi provided helpful comments on a previous draft of this paper. The authors declare no competing interests in the publication of this paper.

BGD
12, 8573–8614, 2015

References

Arino, O., Asner, G., Boschetti, L., Braatz, B., Chiuvieco, E., Csiszar, I., Cutler, M., Englhart, S., de Jong, B., Falkowski, M., Federici, S., Franke, J., Goetz, S., Harris, N., Hirata, Y., Hoekman, D., Hoffman, A., Joosten, H., Justice, C., Kellndorfer, J., Kull, S., Kurz, W., Lambin, E., Lucas, R., McCall, M., McRoberts, R., Monni, S., Moore, R., Naesset, E., Nelson, R., Shimabukuro, E., Paganini, M., Pearson, T., Richards, G., Rosenqvist, A., Roy, D., Russell-Smith, J., Siegert, F., Shoch, D., Skutsch, M., Spessa, A., Van Laake, A., and Wulder, M.: A sourcebook of methods and procedures for monitoring and reporting anthropogenic greenhouse gas emissions and removals caused by deforestation, gains and losses of carbon stocks in forests, remaining forests and forestation, GOFC-GOLD, available at: http://www.gofcgold.wur.nl/redd/ (last access: 8 May 2015), 2009. 8577

Asner, G., Powell, G., Mascaro, J., Knapp, D., Clark, J., Jacobson, J., Kennedy-Bowdoin, T., Balaji, A., Paez-Acosta, G., Victoria, E., Secada, L., Valqui, M., and Hughes, Hughes, F.: High-resolution forest carbon stocks and emissions in the Amazon, P. Natl. Acad. of Sci. USA, 107, 16738–16742, 2010. 8578

Bicheron, P., Defourny, P., Brockmann, C., Schouten, L., Vancutsem, C., Huc, M., Bontemps, S., Leroy, M., Achard, F., Herold, M., Ranera, F., and Arino, O.: Global Land Cover Map Online, available at: http://due.esrin.esa.int/globcover/ (last access: 15 August 2014), 2009. 8584, 8593

Boden, T., Marland, G., and Andres, R.: Global, Regional, and National Fossil-Fuel CO_2 Emissions, department of Energy, Carbon Dioxide Information Analysis Center, Oak Ridge National Laboratory, Oak Ridge, Tennessee, USA, doi:10.3334/CDI-AC/00001_V2010, 2010. 8575

Broich, M., Hansen, M., Potapov, P., Adusei, B., Lindquist, E., and Stehman, S.: Time-series analysis of multi-resolution optical imagery for quantifying forest cover loss in Sumatra and Kalimantan, Indonesia, Int. J. Appl. Earth Obs., 13, 277–291, 2011a. 8579, 8581, 8598

Broich, M., Hansen, M., Stolle, F., Potapov, P., Margono, B., and Adusei, B.: Remotely sensed forest cover loss shows high spatial and temporal variation across Sumatera and Kalimantan, Indonesia 2000-2008, Environ. Res. Lett., 6, 014010, doi:10.1088/1748-9326/6/1/014010, 2011b. 8580, 8581

Bulte, E. and Engel, S.: Conservation of tropical forests: addressing market failure, edited by: Lopez, R. and Toman, M., 412–52, 2006. 8574

BGD
12, 8573–8614, 2015

Chave, J., Condit, R., Aguilar, S., Hernandez, A., Lao, S., and Perez, R.: Error propagation and scaling for tropical forest biomass estimates, Philos. T. Roy. Soc. B, 359, 409–420, 2004. 8583, 8587

Chave, J., Andalo, C., Brown, S., Cairns, M., Chambers, J., Eamus, D., Folster, H., Fromard, F., Higuchi, N., Kira, T., Lescure, J., Nelson, B., Ogawa, H., Puig, H., Riera, B., and Yamakura, T.: Tree allometry and improved estimation of carbon stocks and balance in tropical forests, Oecologia, 145, 87–99, 2005. 8582

Cohen, R.: Estimating the above-ground biomass of mangrove forest in Kenya, PhD thesis, University of Edinburgh, https://www.era.lib.ed.ac.uk/bitstream/handle/1842/9956/Cohen2014.pdf?sequence=1 (last access: 25 May 2015), 2014. 8596

Collins, M., Macdonald, E., Clayton, L., Dunggio, I., Macdonald, D., and Milner-Gulland, E.: Wildlife conservation and reduced emissions from deforestation in a case study of Nantu Wildlife Reserve, Sulawesi: 2. An institutional framework for REDD implementation, Environ. Sci. Policy, 14, 709–718, 2011. 8582, 8593

Diaz, D., Hamilton, K., and Johnson, E.: State of the forest carbon markets 2011: From canopy to currency, The Ecosystem Marketplace, 70 pp., 2011. 8575

Djomo, A., Ibrahima, A., Saborowski, J., and Gravenhorst, G.: Allometric equations for biomass estimations in Cameroon and pan moist tropical equations including biomass data from Africa, Forest Ecol. Manage., 260, 1873–1885, 2010. 8594

Eggleston, H., Buendia, L., Miwa, K., Ngara, T., and Tanabe: Guidelines for National Greenhouse Gas Inventories, 4, 53, 2006. 8587

Gaveau, D.: Nearly a quarter of June fires in Indonesia occurred in industrial plantations, Online, available at: http://blog.cifor.org/18218/research-nearly-a-quarter-of-june-fires-in-indonesia-occurred-in-industrial-plantations (last access: 15 May 2015), 2013. 8581, 8599

Gaveau, D., Epting, J., Lyne, O., Linkie, M., Kumara, I., Kanninen, M., and Leader-Williams, N.: Evaluating whether protected areas reduce tropical deforestation in Sumatra, J. Biogeogr., 36, 2165–2175, 2009. 8579

Grace, J., Mitchard, E., and Gloor, E.: Perturbations in the carbon budget of the tropics, Glob. Change Biol., 20, 3238–3255, doi:10.1111/gcb.12600, 2014. 8574, 8575

Hansen, Matthew, C., Roy, D., Lindquist, E., Adusei, B., Justice, C., and Altstatt, A.: A method for integrating MODIS and Landsat data for systematic monitoring of forest cover and change in the Congo Basin, Remote Sens. Environ., 112, 2495–2513, 2008. 8580, 8597

BGD
12, 8573–8614, 2015

Hansen, Matthew, C., Stehman, S., Potapov, P., Arunarwati, B., Stolle, F., and Pittman, K.: Quantifying changes in the rates of forest clearing in Indonesia from 1990 to 2005 using remotely sensed data sets, Environ. Res. Lett., 4, 034001, 2009. 8580, 8597

Hansen, M. C., Potapov, P. V., Moore, R., Hancher, M., Turubanova, S. A., Tyukavina, A., Thau, D., Stehman, S. V., Goetz, S. J., Loveland, T. R., Kommareddy, A., Egorov, A., Chini, L., Justice, C. O., and Townshend, J. R. G.: High-Resolution Global Maps of 21st-Century Forest Cover Change, Science, 342, 850–853, doi:10.1126/science.1244693, 2013. 8580

Harris, N.: Baseline map of carbon emissions from deforestation in tropical regions, Science, 337, 1573–1576, 2012. 8575

Hijmans, R.: Raster: Geographic data analysis and modeling, http://CRAN.R-project.org/package=raster, R package version 2.1-48, 2013. 8586

Hooijer, A., Page, S., Canadell, J. G., Silvius, M., Kwadijk, J., Wösten, H., and Jauhiainen, J.: Current and future CO_2 emissions from drained peatlands in Southeast Asia, Biogeosciences, 7, 1505–1514, doi:10.5194/bg-7-1505-2010, 2010. 8599

Hooijer, A., Page, S., Jauhiainen, J., Lee, W. A., Lu, X. X., Idris, A., and Anshari, G.: Subsidence and carbon loss in drained tropical peatlands, Biogeosciences, 9, 1053–1071, doi:10.5194/bg-9-1053-2012, 2012. 8599

Houghton, R. A.: How well do we know the flux of Carbon dioxide from land-use change?, Tellus Series B, 62, 337–351, doi:10.1111/j.1600-0889.2010.00473.x, 2010. 8575

IUCN: The IUCN Red List of Threatened Species, version 2013.1., available at: http://www.iucnredlist.org/, last access: 12 May 2013. 8581, 8599

Jaenicke, J., Rieley, J. O., Mott, C., Kimman, P., and Siegert, F.: Determination of the amount of carbon stored in Indonesian peatlands, Geoderma, 147, 151–158, 2008. 8599

JAXA: New global 25m-resolution PALSAR mosaic and Global Forest/Non-forest Map, available at: http://www.eorc.jaxa.jp/ALOS/en/palsar_fnf/data/, last access: 5 August 2014. 8584

Joshi, N., Mitchard, E. T., Woo, N., Torres, J., Moll-Rocek, J., Ehammer, A., Collins, M., Jepsen, M. R., and Fensholt, R.: Mapping dynamics of deforestation and forest degradation in tropical forests using radar satellite data, Environ. Res. Lett., 10, 034014 doi:10.1088/1748-9326/10/3/034014, 2015. 8575

Koh, L. and Sodhi, N.: Conserving Southeast Asias imperiled biodiversity: scientific, management, and policy challenges, Biodivers. Conserv., 19, 913–917, doi:10.1007/s10531-010-9818-9, 2010. 8575

BGD
12, 8573–8614, 2015

Lefsky, M. A.: A global forest canopy height map from the Moderate Resolution Imaging Spectroradiometer and the Geoscience Laser Altimeter System, Geophys. Res. Lett., 37, 2010. 8578, 8583, 8595

Legendre, P.: lmodel2: Model II Regression, http://CRAN.R-project.org/package=lmodel2 (last access: 15 January 2015), R package version 1.7-2, 2014. 8588

Lewis, S. L., Lopez-Gonzalez, G., Sonké, B., Affum-Baffoe, K., Baker, T. R., Ojo, L. O., Phillips, O. L., Reitsma, J. M., White, L., Comiskey, J. a., Djuikouo K, M.-N., Ewango, C. E. N., Feldpausch, T. R., Hamilton, A. C., Gloor, M., Hart, T., Hladik, A., Lloyd, J., Lovett, J. C., Makana, J.-R., Malhi, Y., Mbago, F. M., Ndangalasi, H. J., Peacock, J., Peh, K. S.-H., Sheil, D., Sunderland, T., Swaine, M. D., Taplin, J., Taylor, D., Thomas, S. C., Votere, R., and Wöll, H.: Increasing carbon storage in intact African tropical forests., Nature, 457, 1003–1006, doi:10.1038/nature07771, 2009. 8575

Linkie, M., Chapron, G., Martyr, D. J., Holden, J., and Leader-Williams, N.: Assessing the viability of tiger subpopulations in a fragmented landscape, J. Appl. Ecol., 43, 576–586, 2006. 8599

Lu, D.: The potential and challenge of remote sensing-based biomass estimation, Int. J. Remote Sens., 27, 1297–1328, 2006. 8577

Margono, B., Turubanova, S., Zhuravleva, I., Potapov, P., Tyukavina, A., Baccini, A., Goetz, S., and Hansen, M.: Mapping and monitoring deforestation and forest degradation in Sumatra (Indonesia) using Landsat time series data sets from 1990 to 2010, Environ. Res. Lett., 7, 034010, doi:10.1088/1748-9326/7/3/034010, 2012. 8580

Miettinen, J., Shi, C., and Liew, S. C.: Deforestation rates in insular Southeast Asia between 2000 and 2010, Glob. Change Biol., 17, 2261–2270, doi:10.1111/j.1365-2486.2011.02398.x, 2011. 8581, 8599

Mitchard, E., Saatchi, S., Lewis, S., Feldpausch, T., Woodhouse, I., Sonké, B., Rowland, C., and Meir, P.: Measuring biomass changes due to woody encroachment and deforestation/degradation in a forest-savanna boundary region of central Africa using multi-temporal L-band radar backscatter, Remote Sens. Environ., 115, 2861–2873, 2011. 8585, 8587

Mitchard, E. T. A., Saatchi, S. S., Gerard, F. F., Lewis, S. L., and Meir, P.: Measuring Woody Encroachment along a Forest-Savanna Boundary in Central Africa, Earth Interact., 13, 1–29, doi:10.1175/2009EI278.1, 2009a. 8576, 8577, 8585

Mitchard, E. T. A., Saatchi, S. S., Woodhouse, I. H., Nangendo, G., Ribeiro, N. S., Williams, M., Ryan, C. M., Lewis, S. L., Feldpausch, T. R., and Meir, P.: Using satellite radar backscatter to

BGD
12, 8573–8614, 2015

predict above-ground woody biomass: A consistent relationship across four different African landscapes, Geophys. Res. Lett., 36, L23401, doi:10.1029/2009GL040692, 2009b. 8585

Mitchard, E. T. A., Saatchi, S. S., White, L. J. T., Abernethy, K. A., Jeffery, K. J., Lewis, S. L., Collins, M., Lefsky, M. A., Leal, M. E., Woodhouse, I. H., and Meir, P.: Mapping tropical forest biomass with radar and spaceborne LiDAR in Lopé National Park, Gabon: overcoming problems of high biomass and persistent cloud, Biogeosciences, 9, 179–191, doi:10.5194/bg-9-179-2012, 2012. 8576, 8577, 8579, 8583, 8595

Morel, A., Saatchi, S., Malhi, Y., Berry, N., Banin, L., Burslem, D., Nilus, R., and Ong, R.: Estimating aboveground biomass in forest and oil palm plantation in Sabah, Malaysian Borneo using ALOS PALSAR data, Forest Ecol. Manage., 262, 1786–1798, 2011. 8577, 8583, 8586, 8594

Murdiyarso, D., Donato, D., J, K., S, K., Stidham, M., and Kanninen, M.: Carbon storage in mangrove and peatland ecosystems, CIFOR, Indonesia, doi:10.17528/cifor/003233, 2010. 8582

Naidoo, R., Balmford, A., Costanza, R., Fisher, B., Green, R. E., Lehner, B., Malcolm, T. R., and Ricketts, T. H.: Global mapping of ecosystem services and conservation priorities, P. Natl. Acad. Sci., 105, 9495–9500, doi:10.1073/pnas.0707823105, 2008. 8574

Page, S., Siegert, F., Rieley, J., Boehm, H., Jaya, A., and Limin, S.: The amount of carbon released from peat and forest fires in Indonesia during 1997, Nature, 420, 61–65, doi:10.1038/nature01131, 2002. 8596, 8599

Penman, J., Gytarsky, M., Hiraishi, T., Krug, T., Kruger, D., Pipatti, R., Buendia, L., Miwa, K., Ngara, T., Tanabe, K., and Wagner, F.: Good Practice Guidance for Land Use, Land-Use Change and Forestry, 3.157, 2003. 8587

R Core Team: R: A Language and Environment for Statistical Computing, R Foundation for Statistical Computing, Vienna, Austria, http://www.R-project.org (last access: 20 November 2014), 2013. 8583, 8585

Reyes, G., Brown, S., Chapman, J., and Lugo, A.: Wood Densities of Tropical Tree Species (United States Department of Agriculture), available at: http://www.researchgate.net/publication/237339477_Wood_Densities_of_Tropical_Tree_Species (last access: 29 August 2012), 1992. 8583

Saatchi, S. S., Harris, N. L., Brown, S., Lefsky, M., Mitchard, E. T. A., Salas, W., Zutta, B. R., Buermann, W., Lewis, S. L., Hagen, S., Petrova, S., White, L., Silman, M., and Morel, A.:

BGD
12, 8573–8614, 2015

Benchmark map of forest carbon stocks in tropical regions across three continents, P. Natl. Acad. Sci., 108, 9899–9904, doi:10.1073/pnas.1019576108, 2011. 8578, 8583, 8584, 8588
Shugart, H. H., Saatchi, S., and Hall, F. G.: Importance of structure and its measurement in quantifying function of forest ecosystems, J. Geophys. Res.-Biogeo., 115, 2156–2202, doi:10.1029/2009JG000993, 2010. 8578
Slik, J. W. F., Paoli, G., McGuire, K., Amaral, I., Barroso, J., Bastian, M., Blanc, L., Bongers, F., Boundja, P., Clark, C., Collins, M., Dauby, G., Ding, Y., Doucet, J.-L., Eler, E., Ferreira, L., Forshed, O., Fredriksson, G., Gillet, J.-F., Harris, D., Leal, M., Laumonier, Y., Malhi, Y., Mansor, A., Martin, E., Miyamoto, K., Araujo-Murakami, A., Nagamasu, H., Nilus, R., Nurtjahya, E., Oliveira, Á., Onrizal, O., Parada–Gutierrez, A., Permana, A., Poorter, L., Poulsen, J., Ramirez-Angulo, H., Reitsma, J., Rovero, F., Rozak, A., Sheil, D., Silva-Espejo, J., Silveira, M., Spironelo, W., ter Steege, H., Stevart, T., Navarro-Aguilar, G. E., Sunderland, T., Suzuki, E., Tang, J., Theilade, I., van der Heijden, G., van Valkenburg, J., Van Do, T., Vilanova, E., Vos, V., Wich, S., Woll, H., Yoneda, T., Zang, R., Zhang, M.-G., and Zweifel, N.: Large trees drive forest aboveground biomass variation in moist lowland forests across the tropics, Global Ecol. Biogeogr., 22, 1261–1271, doi:10.1111/geb.12092, 2013. 8594
Solheim, E. and Natalegawa, R.: Letter of Intent between the Government of the Kingdom of Norway and the Government of the Republic of Indonesia, Cooperation on reducing greenhouse gas emissions from deforestation and forest degradation, available at: https://www.regjeringen.no/globalassets/upload/smk/vedlegg/2010/indonesia_avtale.pdf (last access: 1 June 2015), 2010. 8580
The Norwegian Embassy: Norway-Indonesia REDD+ Partnership – Frequently asked questions, available at: http://www.norway.or.id (last access: 15 February 2014), 2011. 8580
UNFCCC: Report of the Conference of the Parties on its seventh session, held at Marrakesh from 29 October to 10 November 2001; FCCC/CP/2001/13/Add.1, available at: http://unfccc.int (last access: 1 October 2014), 2001. 8586
UNFCCC: Appendix 1: Guidance and safeguards for policy approaches and positive incentives on issues relating to reducing emissions from deforestation and forest degradation in developing countries; and the role of conservation, sustainable management of forests and enhancement of forest carbon stocks in developing countries., http://unfccc.int/documentation/documents/advanced_search/items/6911.php?priref=600006173 (last access: 1 October 2014), 2010. 8575

BGD
12, 8573–8614, 2015

van der Werf, G. R., Morton, D. C., DeFries, R. S., Olivier, J. G. J., Kasibhatla, P. S., Jackson, R. B., Collatz, G. J., and Randerson, J. T.: CO2 emissions from forest loss (vol 2, pg 737, 2009), Na. Geosci., 2, 737–738, doi:10.1038/ngeo720, 2009. 8574, 8599

Whitten, A., Anwar, J., Damanik, S., and Hisyam, N.: The Ecology of Sumatra, Oxford University Press, 512 pp., 1984. 8581

Woodhouse, I., Mitchard, E., Brolly, M., Maniatis, D., and Ryan, C.: Correspondence: Radar backscatter is not a "direct measure" of forest biomass, Nature Climate Change, 2, 556–557, 2012. 8576

BGD

12, 8573–8614, 2015

Table 1. Regression equation for relationship between 2007 HV backscatter and the binned Lorey's height data taken from the ICESat dataset.

RMA Regression: PALSAR dB HV to Lorey's height	RMSE	R^2	n
Lorey's height $t = e^{\left(\left(\left(\mathrm{HV}_t^{\mathrm{dB}} + 14.9\right)/0.88\right)\right)}$	3.31 m	0.91	26

BGD
12, 8573–8614, 2015

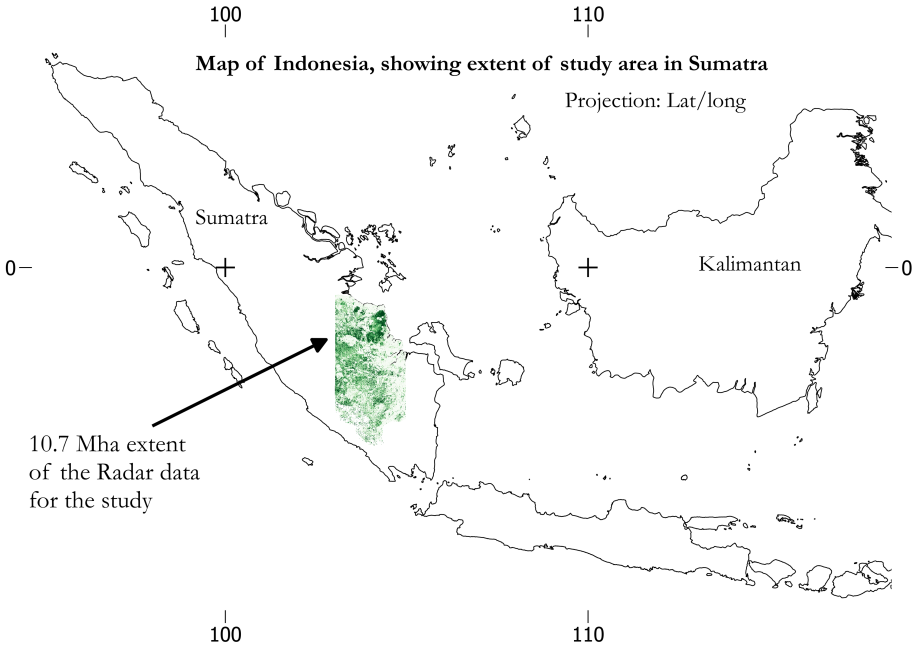

Figure 1. A map of the western islands of the Indonesian archipelago. The island oriented north-west to south-east is Sumatra. The section highlighted is our study area of 10.7 Mha. The underlying data for that section is our estimate of AGB for 2007. Dark greens areas are those with high AGB, and lighter coloured areas have very low AGB. In the northern-most tip of the image is the dark green of Berbak national park, reflecting its relatively intact status. It was from this site that we gathered our field data via ZSL which operates a pilot REDD+ project there. The south of the study area terminates at the Bukit Barisan mountain range.

BGD
12, 8573–8614, 2015

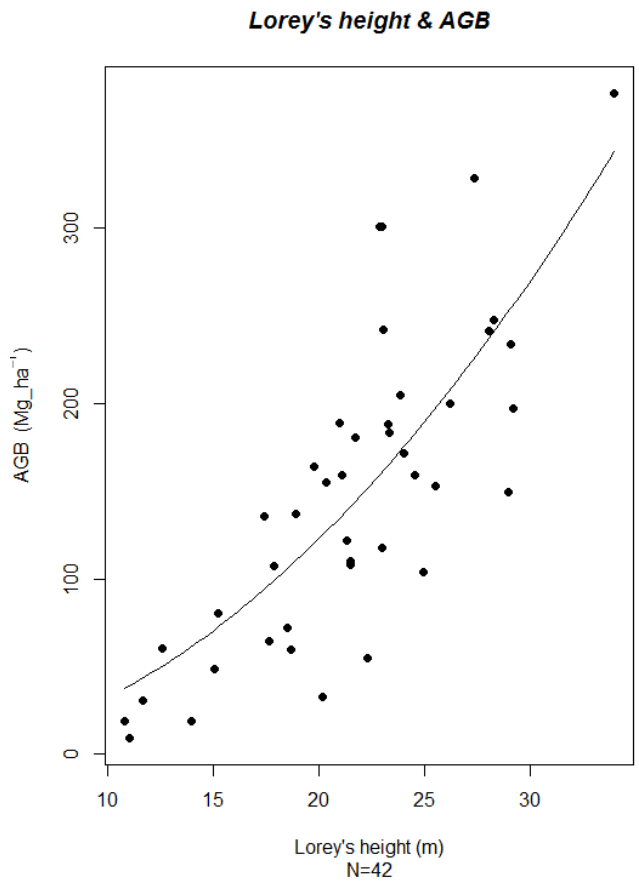

Figure 2. Relationship between Lorey's height and biomass as measured in the forest plot data from Berbak National Park. $R^2 = 0.61$; RMSE = 113 Mg ha^{-1}

BGD
12, 8573–8614, 2015

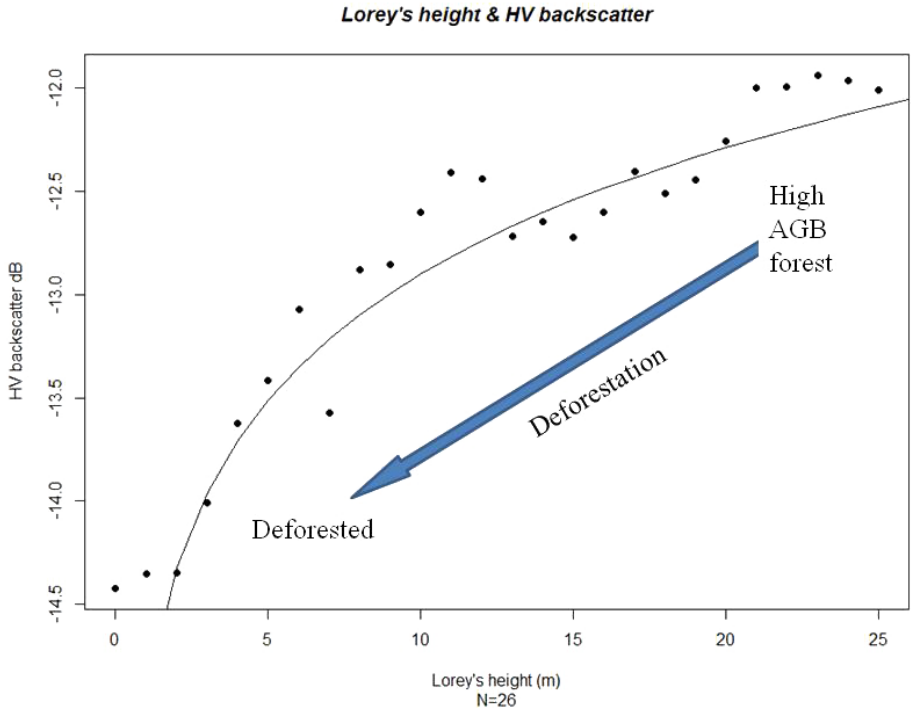

Figure 3. Non-linear relationship between HV backscatter and Lorey's height. This diagram demonstrates the logic behind the selection of the 10 m height threshold for the definition of deforestation. Values in the upper right of the graph have both high Lorey's height values and high HV backscatter values, which we interpret as being natural high biomass forest. In the bottom left of the image are data points which have low AGB and low Lorey's height values, which we interpret as being degraded forest, through to cleared forest. If the value of a pixel moves from the upper right of the plot to the lower left, such that the height reduction is ≥ 10 m during one year, we interpret this as a deforestation event. This process is represented by the arrow pointing downwards to the left.

BGD
12, 8573–8614, 2015

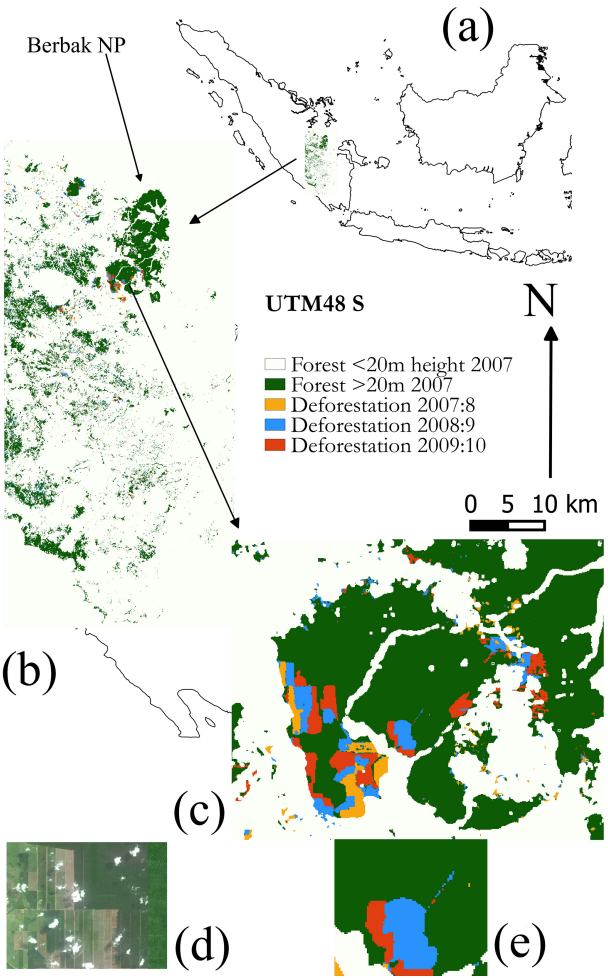

BGD
12, 8573–8614, 2015

Integrated radar and lidar analysis reveals extensive forest biomass change

M. B.Collins and E. T. A. Mitchard

Figure 4. (a) Location of study area on Sumatra, Indonesia. **(b)** Study area. Non-forest and forest of low (< 20 m in 2007) height in grey, which areas are excluded from the analysis; and forest in green (height ≥ 20 m in 2007). Few large blocks of intact forest remain except Berbak national park, obvious as an area of dark green in the far north. The large area in the centre of the park burned in the 1996/7 fires. The "ribbons" of non-forest areas running through the park indicate where we have removed flooded forest. Deforestation after 2007 is yellow, blue, orange for each subsequent year. **(c)** Demonstrates the annual progression of forest loss in large geometric patterns consistent with forest clearance for roads, canals and plantations. **(d)** High resolution GoogleEarth image from 8 May 2009, providing optical verification of changes detected using SAR. This image may be viewed at full resolution in GoogleEarth at 1°53′40.71″ S, 103°52′56.69″ E. **(e)** We are able to detect forest infrastructure development, here a road/canal connecting different areas of plantation.

BGD
12, 8573–8614, 2015

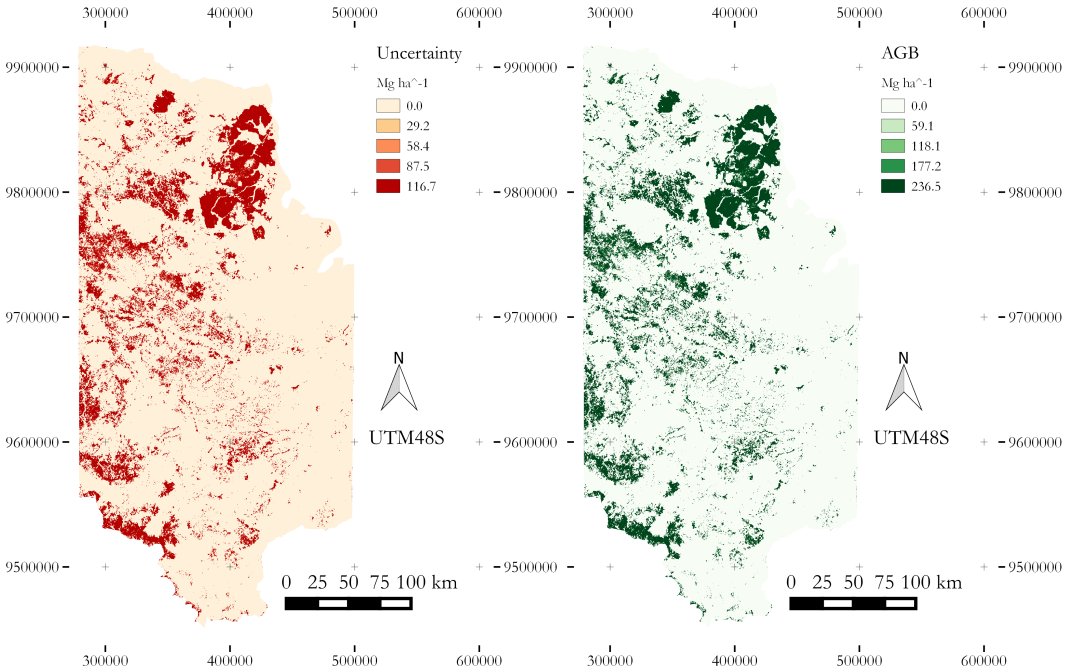

Figure 5. Left image: uncertainty of the 2007 AGB for our 10.7 Mha study area. We created the uncertainty map by applying the 24.7 % total uncertainty across the landscape. Hence those areas which have higher estimates of AGB have the highest absolute uncertainties associated with them.The uncertainties appear to be fairly constant across the landscape because we are considering only the high biomass forests in the analysis. Right image: the AGB map for 2007. The AGB legend is scaled continuously between minimum and maximum values. The largest remaining block of forest in the north-east of the image is Berbak national park, and the forests of ZSL's pilot REDD+ project, the Berbak Carbon Initiative.

BGD
12, 8573–8614, 2015